SIMULATED *ASTER* DATA I OR GEOLOGIC STUDIES

MICHAEL ABRAMS AND SIMON HOOK

JET PROPULSION LABORATORY/
CALIFORNIA INSTITUTE OF TECHNOLOGY
PASADENA, CA

ABSTRACT

The Advanced Spaceborne Thermal Emission and Reflectance Radiometer (ASTER) is a high spatial resolution imaging instrument, due to be launched on NASA's Earth Observing System AM-1 satellite platform in 1998. ASTER acquires data in 14 bands, spanning the wavelength region from the visible, mar infrared, short wave] ength infrared, and thermal infrared, with spatial resoluti on varying from 15 m to 90 m, depending on wavelength region. in order to evaluate our ability to use ASTER data for geological mapping, we used aircraft data over Cuprite, Nevada to create a simulated 14-band ASTER data set. The study site has sparse vegetation, and exposes a wide range of unaltered and hydrothermally altered volcanic recks. The wide range of wavelengths covered by ASTER allowed us to recognize or separate iron oxide minerals, clay-bearing minerals, sulfate minerals, ammonia minerals, siliceous rocks, and carbonates. Combined with laboratory spectral measurements, we were able to identify these constituents. Based on both sets of information, we produced an alteration map showing the distribution of argillized rocks, opalized rocks with alunite, silicified rocks, and areas dominated by kaolinite and buddingtonite. The map was as accurate as published maps made by traditional field methods, ASTER promises to be a major improvement over existing satellite systems for geologic mapping.

INTRODUCTION

Remote sensing data for earth science applications will be greatly improved in 1998 with the launch of NASA's Earth Observation System AM-1 satellite platform, that will carry five earth observation instruments. One of these instruments is the Advanced Spaceborne Thermal Emission and Reflectance Radiometer (ASTER). This imaging system will provide high spatial resolution data in the visible, near infrared, short wave infrared, and thermal infrared wavelength regions (Kahle et al., 1991); and along-track stereo imaging capability for producing digital elevation models. ASTER is a joint project between Japan and the US; the Japanese arc building the instrument, and the US is providing the launch vehicle. and telemetry; science team activities and data distribution are shared responsibilities,

ASTER is the only high-spatial-resolution surface imager on EOS-A. As a result there are a variet y of distinct science objectives for the instrument. The main cent ribut ions to the EOS global change studies will be in providing surface temperatures, surface emitted and reflected radiances, and digital elevation models (DEM 's) at a spatial scale that will allow detailed surface studies to be conducted at the sub-pixel level for other global monitoring instruments.

The multispectral thermal infrared data will provide information to enable better separation of the brightness temperature into surface kinetic temperature and land surface spectral emissivity, than has been possible to date with broad-band thermal imaging instruments. These land surface, temperature data have applications in studies of surface radiation balance as required by climate, weather and biogeochemical models. They can be used to aid in the quantification of evaporation and evapo-transpiration, and the interactions bet wccn veget at ion, soils and the h ydrogeol ogic cycle, Temperature data will be used in the monitoring and analysis of volcanic processes. Day and night

3

temperature data will be used to estimate thermal inertia as an aid to surface compositional mapping.

The extensive wavelength coverage combined with same-orbit stereo capability will contribute to the EOS surface compositional, structural and geomorphological mapping objective which supports or provides a base for local, regional and global geological studies. The visible and near infrared (VNIR) and short wave infrared (S WIR) bands have been chosen specificall y for use in surface compositional mapping. These high spatial resolution data will support, for example, lithofacies mapping and stratigraphic analysis which will contribute to the knowledge of sea level change, coastal erosion, palaeoclimate and the distribution of mineral resources. Soil mapping can contribute to a knowledge of long term and short term changes in soil characteristics, quality and land use. These data can also be used to help monitor and understand how episodic processes such as rainfall, runoff, dust storms, earthquakes and volcanism modify the earth,

The two primary satellite instruments currently acquiring multispectral data for earth science applications arc the Land sat Thematic Mapper (TM) and the SPOT satellite. TM acquires 6 bands of data in the reflected part of the spect rum, and 1 broad thermal channel; SPOT acquires either 3-band visible-near infrared data or a single panchromatic band ('liable 1), Neither instrument has the capability to obtain multispectral data in either the short wavelength infrared or in the thermal infrared parts of the spectrum.

The type of data that ASTER will produce globally arc now available locally using aircraft instruments. in this paper we present an example of the utility of these data for geological surface studies at a well known test site: Cuprite, Nevada. Multi spectral data from two NASA aircraft scanners, the Airborne Visible and Infrared imaging Spect rometer (AVIRIS) and the Thermal

4

infrared Multispectral Scanner (TIMS,) were resampled to the ASTER bands and spatial resolution. The resampled data were analyzed to demonstrate the potential lithologic mapping and discrimination capabilities that ASTER data will provide.

THE ASTER INSTRUMENT

ASTER is a high-spatial-resolution multispectral imager currently scheduled to fly in Earth orbit in 1998 on the first platform of NASA's Earth Observing System (EOS-AM1) (Figure 1). The instrument will have three bands in the visible and near infrared (VNIR) spectral range (0.5-1.0 pm) with 15 m resolution, six bands in the short wave infrared (SWIR) spectral range (1 .0-2,5 pm) with 30 m spatial resolution, and five bands in the thermal infrared (TI R) spectral range (8-12 pm), with 90 m resolution (Fujisada and One, 1991; Kahle et al., 1991) (Table 1). An additional forward viewing telescope with a single band in the near infrared with 15 m spatial resolution will provide the capability, when combined with the. nadir viewing elements, for same-orbit stereo data, The swath width of an image will be 60 km. Cross-track pointing out to 136 km will allow viewing of any spot on Earth at least once every sixteen days. Performance requirements and instrument parameters are shown in Table II.

The instrument is being provided by the Japanese Government under MIT1 (Ministry of International Trade and Industry). The ASTER project is implemented through ERSDAC (Earth Resources Satellite Data Analysis Center) and JAROS (Japan Resources Observation System Organization) which arc non-profit organizations under the control of MIT]. JAROS is responsible for the design and development of the ASTER instrument, which will be carried out by the

Nippon Electric Company (NRC), the Mitsubishi Electric Corporation (ME].(X)), Fujitsu and Hitachi under contracts with JAROS.

STUDY SITE

The Cuprite area is located on the western edge of Esmerelda County, Nevada, about 25 kilometers south of the town of Goldfield. Exposures are very good; vegetation cover varies from 0 to 20%. This study site was selected because of its excellent rock exposures, extensive range of mineral suites, and our and other researchers' long history of remote sensing studies at Cuprite. The first major remote sensing study of the area was by Rowan et al. (1974), who noted the high albedo and iron oxide absorption at Cuprite using the Landsat MSS data. Abrams et al. (1977) compared Landsat MSS data against airborne scanner data with bands similar to those now in place on the Landsat Thematic Mapper. Mineral absorption features reported by Abram et al, (1977) in the 2000 to 2400 nm region led, in part, to the placement of Band 7 (centered on 2200 nm) on the Landsat Thematic M apper. Other remote sensing Studies at Cuprite have included Ashley and Abrams (1 980), Kahle and Goetz (1983), Goetz and Srivastava (1985), and Smith and Adams (1985). More recently, Kruse et al. (1990) reported on the mineral mapping capabilities of a 63 band Geophysical Environmental Research imaging Spectrometer (GERIS); and Hook et al,. (1991) compared the mineral mapping capabilities of the Geoscan MarkII scanner and AVIRIS.

The geologic map of the study area (Figure 2) shows extensive exposure of Tertiary volcanic rocks, and Quaternary deposits (alluvium and playa). Sections of the Tertiary volcanic rocks were intensively altered by a hydrothermal system during mid- to]ate-Miocene time. Ashley and Abrams (1980) divided the hydrothermal alteration into three field - mappable zones: si licified

6

rocks, opalized rocks (opalite), and argillized rocks (Figure 3). The alteration has a bullseye pattern, with the silicified zone forming a circular core surrounded by opalized and then argillized rocks (Figure 3). The following descriptions of the alteration zones is based on those given by Ashley and Abrams (1980).

The silicified rocks are the most intensively alteı cd portions of Cuprite and typically contain abundant quartz, calcite and minor alunite and kaolinite. The opalized rocks form the most widespı cad alteration zone and consist of opaline silica with variable amounts of alunite anti kaolinite with minor calcite, The argillized rocks are the least abundant style of alteration and occur locally with the opalized rocks or at the edges of the alteration area (Figure 3); plagioclase is altered to kaolinite, and mafic minerals are altered to hematite and goethite. The distribution of the.sc alteration assemblages is characteristic of a fossilized hot-spring deposit (e.g. Buchanan, 1981). These hot-spring deposits frequently contain gold mineralization and their recognition is import ant for mineral exploı ation. Buchanan (198 1) provides descriptions of similar deposits. in addition to the alteration minerals already described, an ammonium feldspar known as buddingtonite has also been identified at Cuprite using high spectral resolution image data from the 2.0 to 2.45 μm range (Goetz and Srivastava, 1985). This mineral is also characteristic of fossil ized hot-spring deposits (Krohn and Altaner, 987).

DATA PREPARATION AND PROCESS] NG FOR ASTER S1 MU] ATION

Two aircraft multispectral scanner data sets were used to produce a simulated ASTER data set for part of the Cuprite area. The two data sets were acquired by NASA's Airborne Visible. and infrared Imaging Spectrometer (AVIRIS) and Thermal Infrared Multi spectral Scanner (TI MS).

AVIRIS data were acquired on July 10, 1992 from the ER-2 aircraft platform. This instrument obtains 212 bands of data in the 0.4 to 2.45 pm; each band is .09 µm wide. The images have an instantaneous field of view (IFOV) of 20 m, and a swath width of about 11 km (Vane, 1987). TIMS data were acquired on July 19, 1991, from the C-130 aircraft. TIMS obtains six bands of data in the 8-12 µm region (center wavelengths at 8.407 µm, 8.801 pm, 9.204 µm, 9.933 pm, 1().703 µm, 11.625 µm). The images have an IFOV of about 20 m and a swath width of about 15 km (Palluconi and Meeks, 1985). Both data sets were provided as instrument perceived radiance by the TIMS and AVIRIS processing facilities,

Initially the aircraft data were spectrally resampled to the ASTER bands. For AVIRIS data, this involved averaging several bands to produce each ASTER band using the full-width-half-maximum values for the ASTER filter functions. Because the TIMS wavelength bands are almost identical to ASTER'S TIR bands, no spectral resampling was necessary. However, since TIMS has 6 bands and ASTER has 5, TIMS band 4 was not used for this simulation. The next step was to register the two data sets to a common, topographic base, using the USGS 1:24,000 maps. The smaller area covered by AVIRIS data became the common area extracted from the TIMS data; the dimensions of the area covered by the simulated ASTER images are 6.6 km E-W, and 9.8 km N-S. Finally, the data were spatially resampled to produce the appropriate pixel size for the three ASTER telescopes (15 m for the VNIR, 30 m for the SWIR, and 90 m for the TIR). This resulted in a VNIR data set of 440 x 652 pixels; a SWIR data set of 220 x 326 pixels; and a TIR data set of 110 x 163 pixels.

The first products produced were simple three-band color additive composites from each of the three wavelength regions. These are shown in Figure 4, in the top row. The left image displays

VNIR bands 3, 2 and 1; the center image displays SWIR bands 4, 6 and 9; and the right image displays TIR bands 13, 12 and 10. These bands in each color composite were displayed as red, green, and blue respectively; the images were linearly contrast stretched prior to photographic playback. Pixel replication was used for the SWIR and TIR images to make the data sets the same size as the VN1 R image. The differences in appearance of smal I details between 15, 30, and 90 m spatial resolution arc clearly apparent. in order to enhance the color information (hence spectral information) in these three composites, the same three band combinations were computer processed using a decorrelation stretch algorithm (Figure 4, bottom row). This procedure exaggerates color saturation, while minimizing shifts in hue (Soha and Schwartz, 1978; Gillespie et al., 1986). Colors in the resulting image can be interpreted in terms of the spectral characteristics of the surface materials, because the relative hues arc still preserved. It should be noted that the imagery presented in Figure 4 was not corrected for atmospheric effects,

To better evaluate the spectral information contained in the ASTER SWIR and TIR bands, wc extracted and plotted image and laboratory spectra for selected rock t ypes. The S WI R image data from which the spectra were extracted were processed to suppress effects due to topography, atmosphere, and solar illumination. There arc two basic approaches to accomplish this: those that u sc parameters derived from the data set itself; and those that require the input of additional information (Cone] et al., 1987). The first of these approaches includes the flat field correction (Roberts et al., 1 986), internal average relative reflectance (Kruse et al., 1990) and log residuals (Green and Craig, 1985). The second includes calibration using reflectance spectra of calibration targets (Conel et al., 1987) and correction using solar-atmospheric models and local atmospheric measurements (Rast et al., 1 991), We chose the flat field method, which operates without a priori

9

data. in practice, an area of the unaltered tuffs was outlined, and the average radiance, was
calculated, Next, each pixel in the image was divided by this average, band by band, to produce
relative. reflectance, This method compensates for multiplicative terms, but does not compensate
for additive terms, In the SWIR region, most of the effects due to the atmosphere are
multiplicative, so the method is suitable; it is not, however suitable for the VNIR where the
atmospheric effects occur as both multiplicative and additive terms.

The calibrated TIR data were corrected for atmospheric effects to radiance at the surface
using the MODTRAN radiative transfer model (Berk et al., 1989). MODTRAN derives values for
the atmospheric correction based on an input atmospheric profile. This profile may be obtained
from a set of default profiles in MODTRAN or replaced with local atmospheric data, In this study
the default mid latitude summer profile was used for the atmospheric values above 5km and local
atmospheric data, acquired from an airsonde launched approximately 30 minutes prior to the
overflight, were used for the values of the input profile Mow 5km. This approach is discussed
more ful l y in Hook et al., (1992) with the LOWTRAN atmospheric model.

The ground radiance data consist of temperature and emissivity information; in this study we
were interested in the emissivity information and relative emissivity variations were extracted from
the data using the alpha residual technique (Kealy and Hook, 1993). The alpha residual data have
the. same spectral shape as emissivity spectra but arc normalized to zero.

ANALYSIS AND DISCUSSION

in the 3-2-1 decorrelation stretch image, Stonewall playa is blue, indicating higher relative.
reflectance in the shortest wavelength band; this is primarily due to a high contribution by

atmospheric scattering over the bright, spectrall y flat playa material. No atmospheric corrections have been applied to these data, so the contributions due to Raleigh scattering are still present in the data. The orange-yellow colored areas expose iron oxide minerals, dominantly hematite, found in the argillized zone. This color is a result of the primary iron conduction band in the ultraviolet that produces a fall-off in reflectance towards short wave] engths (Hunt et al., 1971a); thus the blue color (band 1) is suppressed, and orange-yellow (red+green) predominate. Small bright blue areas within the opalized zone are open pits mined for alunite. The bright blue color indicates high albedo, and relatively high atmospheric scattering at short wavelengths, similar to the playa. The majority of the opalized zone, and the silicified zone are. purple colored; this results from a combination of high reflectance due to atmospheric scattering in band 1, and relatively high reflectance in band 3, typical of high albedo altered rocks (Abram and Ashley, 1977). Unaltered rocks, including basalt, tuffs, and alluvial fans derived from them, appear dark blue or black; this is due to their low albedo and lack of major spectral absorption features.

]n the right half of Figure 5 arc shown selected laboratory reflectance spectra in the 2 to 2.4 pm wavelength region for materials from Cuprite, resampled to the ASTER bands; the center wavelengths of each of the ASTER SWIR bands arc also shown by the square data points. On the. left side of the figure are single pixel image spectra extracted from the simulated ASTER data. The method of processing the data to compensate for atmospheric effects was described earlier.

in the 4-6-9 decorrelation stretch image (Figure 4, bottom row center) unaltered rocks (the playa and exposures of tuff) appear in blue colors, indicating they arc spectrally flat, and have higher relative reflectances in band 9. The basalt outcrop west of the highway appears black due to its very low al bedo in the SWIR. The opalized zone appears in yellow-green colors; this is due to

11

a high reflectance in band 4 (the red component), moderate absorption in band 6, and moderate reflectance in band 9. The position of band 6 is on the shoulder of the major alunite absorption feature, centered at 2.15 µm (Figure S), which is a combination of the fundamental OH stretch and Al-O-H bends (Hunt et al., 197 lb), and is not greatly affected by it, Kaolinite Hill appears red-pink in color, due to the suppression of the blue component from the fundamental Al-OH absorption feature at 2.22 µm in band 6 (Hunt et al., 1970), relatively low reflectance in band 9 due to the fundamental OH absorption band at 2..7 µm, and high reflectance in band 4 (Figure 5). Rocks in the silicified zone appear in two colors: an inner blue area, and an outer purple area. Reports by Podwysocki et al. (1986) of a strong Si-OH absorption feature at 2.25 µm in hydrothermal silica may be responsible for the color (Figure 5). Absorption in band 6 reduces the green component, and produces a purple color in the outer silica zone. The blue color of the central zone suggests this same absorption feature, and additionally either a higher value in band 9 or lower value in band 4. Further field sampling is necessary to support this conclusion. Smal 1 exposures of buddingtonite appear pink-purple in color, due to the relatively high reflectance in bands 4 and 9, and the absorption feature near band 6 (Figure 5).

For the TIR bands, we have displayed ASTER bands 13-12-10 (lower right, Figure 4); this is equivalent to the decorrelation stretched TIMS 5-3-1 band combination, used by Kahle and Goetz (1983), for display of lithologic information. For comparison Figure 6 (right) shows field emissivit y spectra for selected materials from Cuprite. These are derived from radiance measurements made with the JPL Field Emission Spectrometer developed by Designs and Prototypes that were resampled to the ASTER wavelengths using the appropriate system response functions. The right plot in Figure 6 shows emissivity, the left plot shows the. alpha residual

spectra. The spectra have been offset vertically for clarity. The center positions of the 5 ASTER TIR binds arc indicated by the square data points for each spectrum. Spectrum A is from a basalt outcrop west of highway 95; spectrum B is from the same opalized/alunite area where we extracted the SWIR spectrum; spectrum C is from the same outcrop of kaolinite as the SWIR spectrum; spectrum D is from the central, silicified area, the same as the SW] R spectrum.

On the decorrelation stretched image, unaltered materials arc in blue, including the playa, tuffs, and the basalt west of the highway; the color is consistent with an absence or low amounts of silica (high values around 8.5 pm). Rocks in the silicified zone arc displayed in yellow-orange. The color is due to an emissivity absorption in band 10 from the primary Si-O stretching in the silicate lattice, called the restrahlen band (Hunt, 1980). The opalized zone, dominated by the presence of alunite, appears in dark purple. The color is due to a strong, broad emission band centered at about 9.5 pm, in ASTER band 12, reducing the green component of' the composite. In the upper left side of the image, a green-yellow area corresponds to outcrops of carbonate; the color is due to the absorption band from bending modes of the carbonate ion occurring at 11.25 pm (Sal isbury et al., 1987).

Based on the spectral analyses presented above, we created a simplified interpretation map showing the. distribution of alteration t ypes (Figure 7). This map was produced by combining information extracted from the simulated ASTER images from all three wavelength regions. We. were able to recognize unaltered rocks, two kinds of silicified rocks, opalized rocks with alunite, argil Ii zed rocks dominated by iron oxides, rocks with dominantly kaolinite present, and outcrops of buddingtonite. This map compares favorably with the field-derived alteration map shown in Figure 3. Ashley and Abrams (1980) defined three types of alteration assemblages: silicified, opalized,

13

and argillized, based on laboratory mineralogical analyses of field samples. The discovery of buddingtonite was based on work with high spectral resolution scanner data; the small size of the outcrops, and the lack of any distinguishing or diagnostic field appearance of buddingtonite prevented its identification from field work, The main difference in our interpretation is the level of detail shown on our map; for publication, wc have simplified small-scale details, and generalized the distribution of small outcrops. In reality, a more detailed map could be produced, at least commensurate with a scale of about 1:50,000, reflecting the inherent detail allowed by ASTER'S spatial resolution (better in the visible, worse in the TIR).

This analysis benefitted from our collection and 1 aboratory measurements of field samples. Using this ancillary information, we were able to identify minerals and mineral assemblages present in the different alteration zones, and then correlate this composition with their spatial distribution in the images. Without this additional data, our interpretation map would still show the same boundaries. However, assigning precise mineralogical identification to the various units would not have been possible. Due to the relatively broad spectral interval of the ASTER bands, unique. mineral identification will not be possible. Rather, classes of minerals will be able to be identified. For example, wc will not be able to differentiate between kaolinite and illite, nor between dolomite and calcite. These separations require spectral resolution of about 5-10 microns to detect the. shifts of characteristic absorption features. However, this is a major improvement over 1.andsat data, where the single band at 2.2 pm only allows the analyst to infer the presence of a clay or carbonate. By comparison, with ASTER data wc will be able to identify the presence of carbonates, iron oxides, smectite minerals, etc.

CONCLUSIONS

ASTER is a 14 band imaging instrument, scheduled for launch as part of the EOS AM platform in 1998. It is the first satellite-borne multispectral scanner incorporating bands throughout both the reflectance and emittance parts of the. electromagnetic spectrum. It will have applications in a wide range of earth observation studies, ranging from ecosystem studies to glaciology. in this paper, we have used simulated ASTER data to examine. the geologic mapping capability over an arid, hydrothermally altered region. We find that information from the 3 wavelength regions is complementary, allowing improved separation and limi ted ident ificat ion of mineralogical assemblages, compared to existing satellite data, such as Landsat Thematic Mapper or SPOT. The VNIR data arc sensitive to the presence of iron oxide minerals; the SWIR data highlight the presence and differences of minerals with hydroxyl radicals and carbonates, such as clays, alunite, and limestone; the TIR data arc sensitive to differences in silica-bearing rocks, either in the presence of or in the absence of the other mineral constituents. Using Landsat TM data, it is on] y possible to identify iron oxides, and detect the presence. of clay-type minerals; no information is avail able related to silica variations. By combining inferred mineralogical information from the 3 ASTER wavelength regions, alteration assemblages can be identified and mapped. This capability is far more efficient than from standard field-based mapping; with the addition of limited field sampling and laboratory anal yscs, these data can be used to produce excellent geologic maps, at a significant savings with respect to time.

ACKNOWLEDGMENTS

REFERENCES

Abram, M., Ashley, R., Rowan, L., Goetz, A., Kahle, A., 1977, Mapping of hydrothermal alteration in the Cuprite mining district, Nevada using aircraft scanner images for the spectral region 0.46 to 2.36 pm: Geology, S, 713-718.

Albers, J., Stewart, J., 1972, Geology and Mineral Deposits of Esmerelda County, Nevada: Nevada Bureau of Mines and Geology, Bulletin 78.

Ashley, R.P. and M.J. Abram, 1980, Alteration Mapping Using Multispectral Images - Cuprite Mining District, Esmerelda County, Nevada: U.S. Geological Survey Open File Report 80-367.

Berk, A., Bernstein, 1.., Robertson, D., 1989, MODTRAN: A moderate resolution model for LOWTRAN 7: GL-TR-89-01 22.

Buchanan, L, J., 1981, Precious Metal Deposits Associated With Volcanic Environments in the Southwest: In W.R. Dickinson and W. Il. Payne. (editors), Relat ions of Tectonics to Ore Deposits in the Southern Cordillera: Arizona Geological Society Digest, 24, 237-262.

Cone], J., Green, R., Vane, G., Bruegge, C., Alley, R., 1987, Airborne. imaging Spectrometer-2: radiometric and spectral characteristics and comparison of ways to compensate for the atmosphere: Proc. SPIE Conf. Imag. Spectros. 1 I.

Fujisada, H., Ono, M., 1991, Overview of ASTER design concept: Proc. SPIE, 1490, .

Gillespie, A., Kahle, A., Walker, R., 1986, Color enhancement of highly correlated images: 1. Decorrelation stretches and HSI contrast Stretches: Remote Sensing of Environment, 20, 209-35.

Goetz, A. and Srivastava, V., 1985, Mineralogical mapping in the Cuprite mining district: Proc. of the First A IS Workshop, Jet Propulsion Laboratory Publication 85-41, 22-31.

Green, A., and Craig, M., 1985, Analysis of aircraft spectrometer data with logarithmic residuals: Proc. First AIS Workshop, Jet Propulsion Laboratory Publication 85-41, 111-119.

Hook, S., Elvidge, C., Rast, M., Watanabe, H., 1991, An evaluation of short-wave-infrared (SWIR) data from the AVIRIS and GEOSCAN instruments for mineralogical mapping at Cuprite, Nevada: Geophys., 56, 1432-1440.

Hook, S., Gabell, A., Green, A., Kealy, P., 1992., A comparison of techniques for extracting emissivity information from thermal infrared data for geologic st udies: Rem. Sens. Environ., 42, 123-135.

Hunt, G., 1980, Electromagnetic radiation: the communication link in remote sensing, in: Remote Sensing in Geology (13. Siegal and A. Gillespie, Ills.), Wiley, pp. 5-45.

Hunt, G., Salisbury, J., Lenhoff, C., 1970, Visible and mar-infrared spectra of minerals and rocks: 1, Silicate minerals: Modern Geology, 1, 283-300.

Hunt, G., Salisbury, J., Lenhoff, C., 1971a, Visible and near-infrared spectra of minerals and rocks: 111. Oxides and hydroxides: Modern Geology, 2, 195-205.

Hunt, G., Salisbury, J., Lenhoff, C., 1971 b, Visible and mar-infrared spectra of minerals and rocks: IV: Sulphides and sulfates: Modern Geology, 3, 1-14.

Kahle, A., Goetz, A., 1983, Mineralogical information from a ncw airborne thermal infrared multispectral scanner: Science, 222, 24-27.

Kahle, A., Palluconi, F., Hook, S., Realmuto, V., Bothwell, G., 1991, The Advanced Spaceborne Thermal Emission and reflectance Radiometer (ASTER): Int. J. Imag. Syst. Tech., 3, 144-156.

Kealy, P., Hook, S. J,, 1993. Separating temperature and emissivity in Thermal Infrared Multi spectral Seamer Data: implications for Recovering Land Surface Temperatures: IEEE Trans. Geosci. and Rem. Sens., 31, 115 S-1 164.

Krohn, D., Altaner, A., 1987, Near-infrared detection of ammonium minerals: Geophys., S2, 924-930.

Kruse, F., Kierein-Young, K., Boardman, J., 1990, Mineral Mapping at Cuprite, Nevada with a 63-Band imaging Spectrometer: Photogram. Eng. and Rem. Sens., 56, 83-92.

Palluconi, F., Meeks, G., 1985, Thermal Infrared Multi spectral Seamer (TIMS): an investigator's guide to TJMS data: Jet Propulsion Laboratory Publication 85-32, Pasadena, CA.

Podwysocki, M., Salisbury, J., Verge, N., 1985, Use of near-infrared spectra to distinguish between sedimentary cherts and hydrothermal silica associated with disseminated gold deposits: 98th Ann. Mtg. Geol. Sot. Amer.

Rast, M., Hook, S., Elvidge, C., 1991, An evaluation of techniques for extraction of mineral absorption feat ures from high spectral resolution remote sensing data: Photog. Eng. Rem. Sens., 57, 1303-1309.

Roberts, D., Yamaguchi, Y., Lyon, R., 1986, Calibration of airborne imaging spectrometer data to percent reflectance using field spectral measurements: Proc. 19th Int. Symp. Rem. Sens. Environ., Ann Arbor, Ml.

Rowan, 1.., Wetlaufer, P., Goetz, A., Billingsley, F., Stewart, J., 1974, Discrimination of Rock Types and Detection of H ydrothermal l y Altered Areas in South-Central Nevada by the Usc of Computer Enhanced ERTS Images: U.S. Geological Survey Professional Paper 883.

Salisbury, J., Walter, L., Verge, N., Mid-infrared (2.1-25 μm) spectra of minerals: U.S. Geological Survey Open-File Report 87-263.

Soha, J., Schwartz, A., 1978, Multi spectral histogram normalization contrast enhancement: Proc. of the Canadian Symp. on Rem. Sins., Victoria, B.C., Canada, 86-93.

Smith, M., Adams, J., 1985, interpretation of AIS images of Cuprite, Nevada using constraints of

spectral mixing: Proc. First AIS Workshop, Jet Propul. Lab. Pub. 85-41, Pasadena, CA.

Vane, G., (cd,), 1987, Airborne visible/infrared imaging spectrometer (AVIRIS): JPL Pub], 87-38, Jet Propul. 1.ab, Pasadena, CA

Fig. 1. Artist's rendition of ASTER instrument on the EOS-A platform,

Fig. 2. Geologic map of the Cuprite, Nevada study site. Redrawn from an unpublished map by R.P. Ashley and map contained in Ashley and Abram (1980). Descriptions of the geologic units have been taken from Albers and Stewart (1972) and the unpublished map by Ashley.

Fig. 3. Alteration map of the Cuprite, Nevada study site. Redrawn from an unpublished map by R.P. Ashley. Map contained in Ashley and Abrams (1980). Numbers and letters refer to sample locations used to obtain image spectra. 1,B=alunite; 2, C=kaolinite; 3=buddingtonite; 4,D= silicified; A=basalt;

Fig. 4, Linear] y (2%) stretched (top row) and decorrelat ion stretched (bottom row) color composites of simulated ASTER data, The left images display bands 3, 2 and 1 in red, green and blue (RGB); the center images display bands 4, 6 and 9 in RGB; and the right images display bands 13, 12 and 10 in RGB. The central wavelengths of these bands are. given in Table 1.

Fig. 5. Reflectance spectra of 4 localities at Cuprite for the 2.0 to 2.4 µm wavelength region. (Left) Single pixel image spectra extracted from flat-field normalized AVIRIS data resampled to the ASTER bands. Locations are shown in Figure 3. (Right) Laboratory spectra measured on a Beckman UV5240 spectrometer in hemispherical reflectance mode, and resampled to the. ASTER SWIR bands. The

locations of central values of the ASTER bands 4 through 9 arc indicated by the square data points. The spectra have been offset vertical] y for clarity. 1=alunite; 2=kaolinite; 3=buddingtonite; 4=silicified.

Fig. 6. Field and image emissivity spectra, resampled to the ASTER TIR bandpasses, of 4 localities at Cuprite for the 8 to 11.5 μm wavelength region, (1 cft) Single pixel image spectra extracted from alpha residual processed ASTER simul ator data. Locati ons arc shown in Figure 3. (Right) Emissivit y spectra derived from JPL's field emission spectrometer, resampled to ASTER wavelengths. The central values of ASTER bands 10 through 14 arc indicated by the square data points. The spectra have been offset vertically for clarity. A=basalt; B=opalized/alunite; C=kaolinite; D=silicified.

Fig. 7. Simplified alteration map of Cuprite interpreted from simulated ASTER data, U=unaltered; A=argillized; P=opalized with alunite; K=dominantl y kaolinite; S 1, S2=silicified; B=buddingtonite.

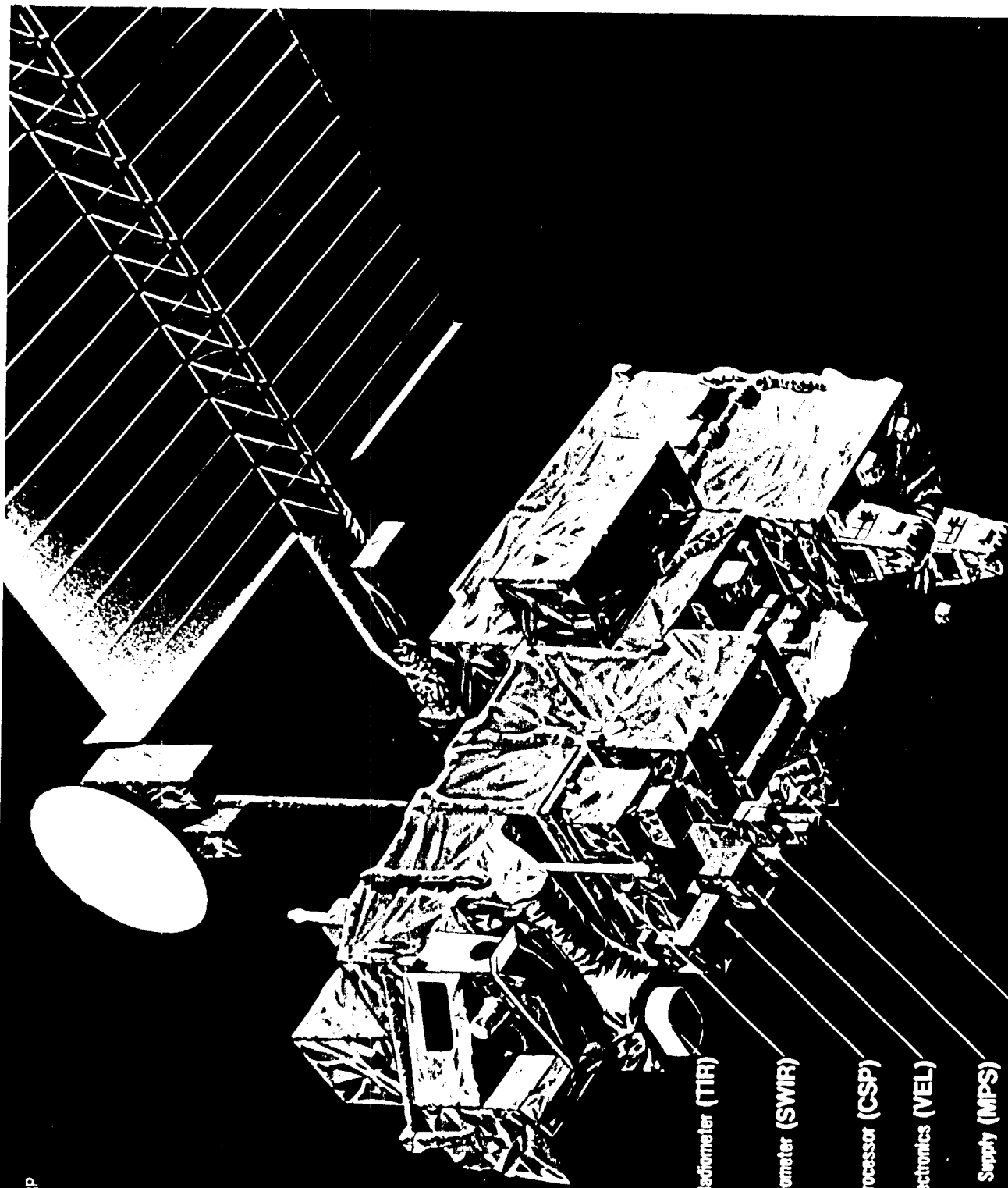Table 1. Spectral Bandpasses, in micrometers

Subsystem	ASTER Band	ASTER Spectral Range	Landsat TM Band	Landsat TM Spectral Range	SPOT Band	SPOT Spectral Range
			1	0.45-0.52		
VNIR	1	0.52-0.60	2	0.52-060	1	0.50-0.59
	2	0.63-0.69	3	0.63-0.69	2	0,61-0.68
	3	0.76 -0.86*:	4	0,76-0.90	3	0.79-0.89
SWIR	4	1.60-1.70	5	1.55-1,75		
	5	2.145-2.185				
	6	2.185-2.225				
	7	2.235-2.285	7	2.08-2.35		
	8	2.295-2.360				
	9	2.360-2.430				
T]R	10	8.125-8.475				
	11	8.475-8.825				
	12	8.925-9.275	6	10.4 -12.5		
	13	10.25-10.95				
	14	10.95-11.65				

*All bands are included in the nadir telescope. This band is replicated in the forward looking telescope.

23

Table II. Overall Performance Requirements

Spatial Resolution	15m Bands 1-3 (VNIR) 30m Bands 4-9 (SWIR) 90m Bands 10- 4 (IR
Stereo Base-to-Height ratio	0 , 6 (Band 3)
Swath Width	60 km (All Bands)
Total edge-to-edge coverage. capability in cross track direction	± 136 km (All Bands)
Cross- track pointing capability (array center)	± 8.54° (All bands)
Signal Quantization	8 bits (Bands 1-9) 12 bits (Bands 10-14)
Modulation Transfer Function (MTF)	0.2?5 (All Bands)
Peak data rate	89.2 Mbps (all bands inducting stereo)
Mission Life	5 years
Mass	352 Kg
Maximum Power	650 W
Physical size	1.6 x 1.6 x 0.9 m

24

Earth Observing System AM-1 Spacecraft (EOS-AM1)

Thermal Infrared Radiometer (TIR)
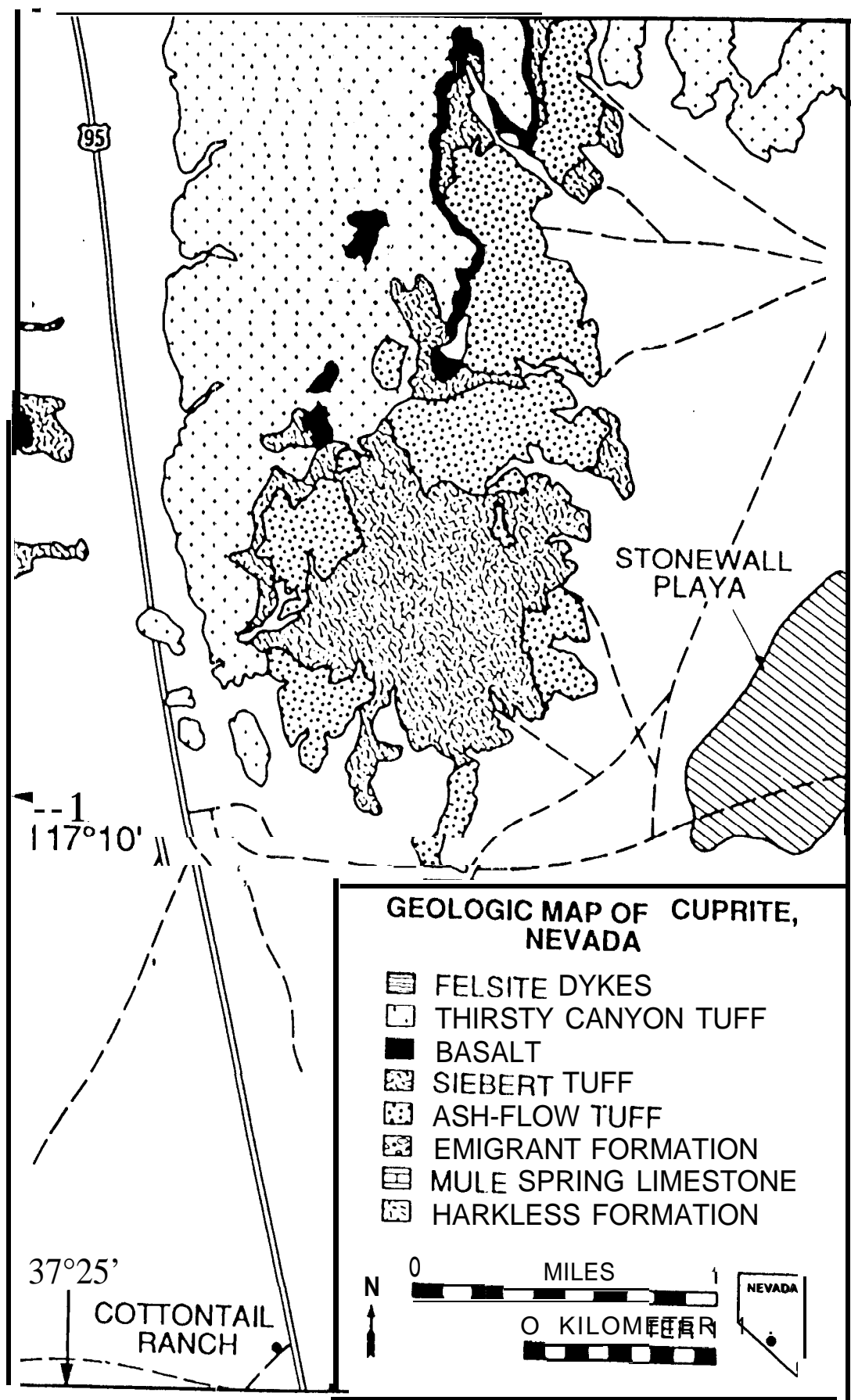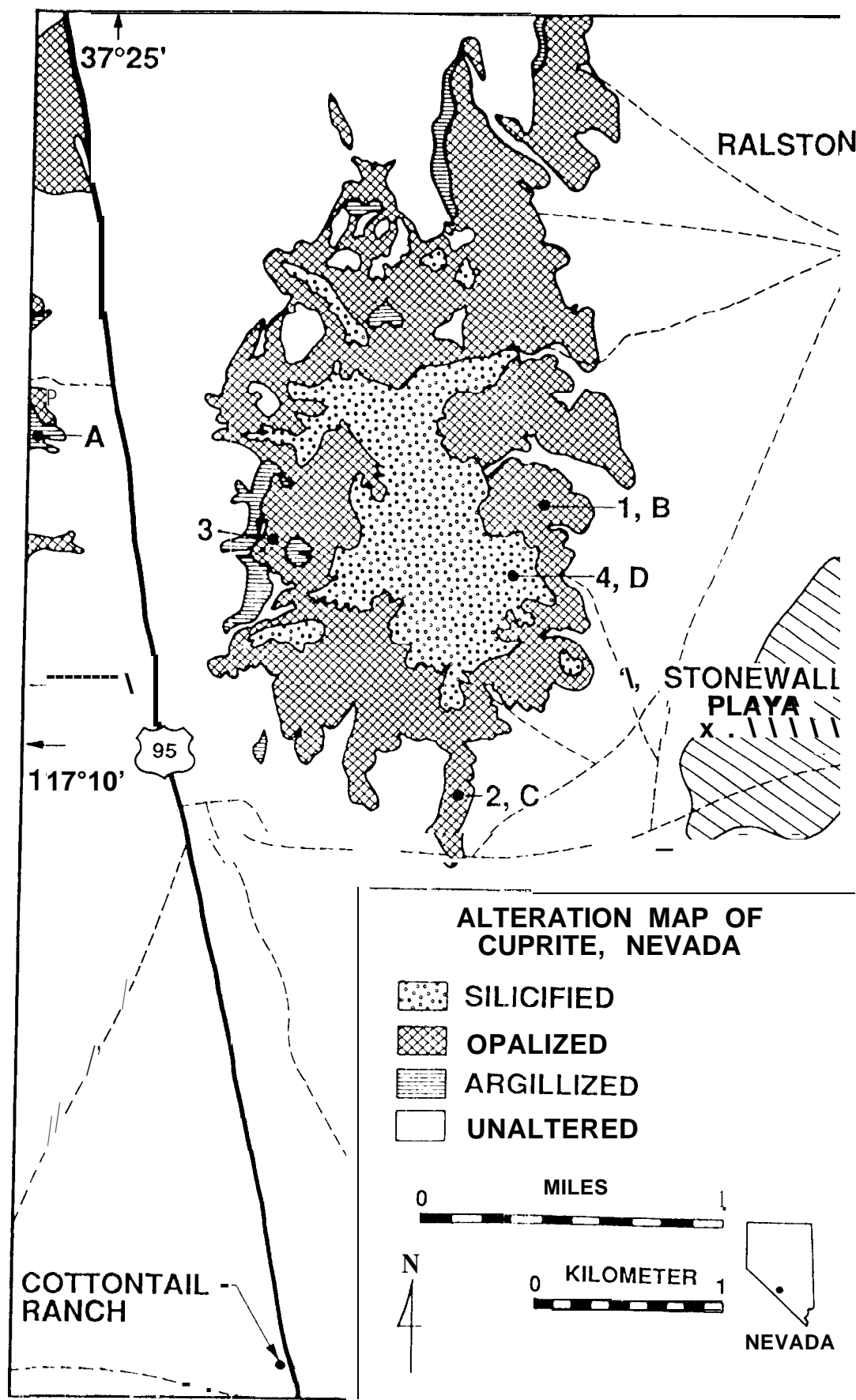
Short-Wave Infrared Radiometer (SWIR)

Common Signal Processor (CSP)

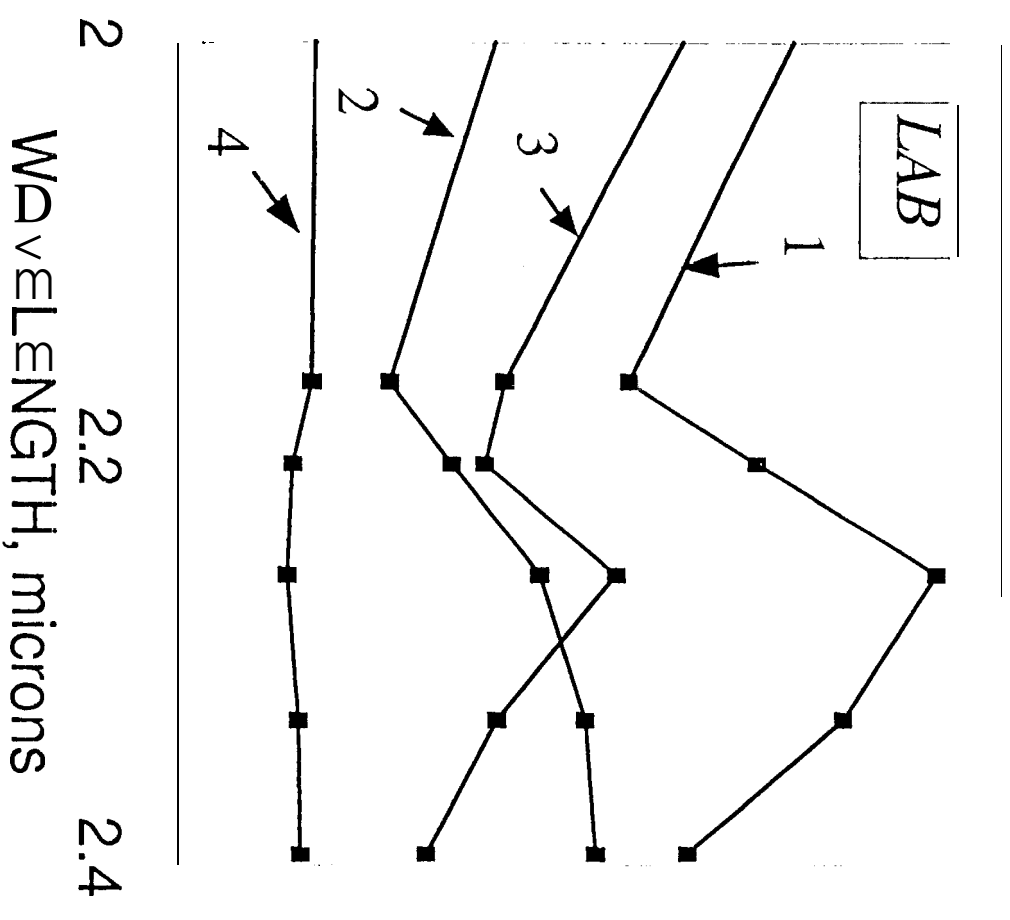Visual and Near Infrared Electronics (VEL)
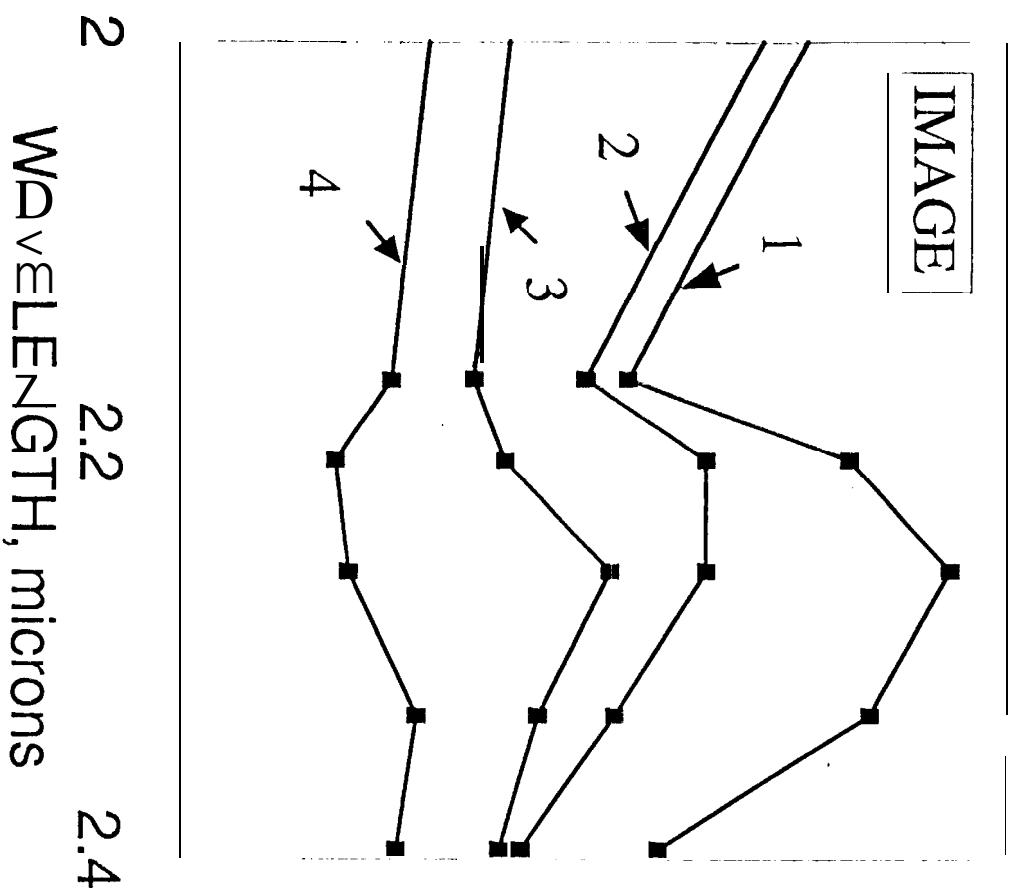
Master Power Supply (MPS)

Visual and Near Infrared
Scanning Radiometer (VSR)

IMAGE COURTESY OF NEC CORP

GEOLOGIC MAP OF CUPRITE, NEVADA

- ▦ FELSITE DYKES
- ▢ THIRSTY CANYON TUFF
- ■ BASALT
- ▨ SIEBERT TUFF
- ▨ ASH-FLOW TUFF
- ▨ EMIGRANT FORMATION
- ▤ MULE SPRING LIMESTONE
- ▨ HARKLESS FORMATION

STONEWALL PLAYA

95

117°10'

37°25'

COTTONTAIL RANCH

N

0   MILES   1

O KILOMETER

NEVADA

ALTERATION MAP OF
CUPRITE, NEVADA

SILICIFIED

OPALIZED

ARGILLIZED

UNALTERED

MILES
0   1

N

KILOMETER
0   1

NEVADA

IMAGE

1
2
3
4

WAVELENGTH, microns

2   2.2   2.4

LAB

1
2
3
4

WAVELENGTH, microns
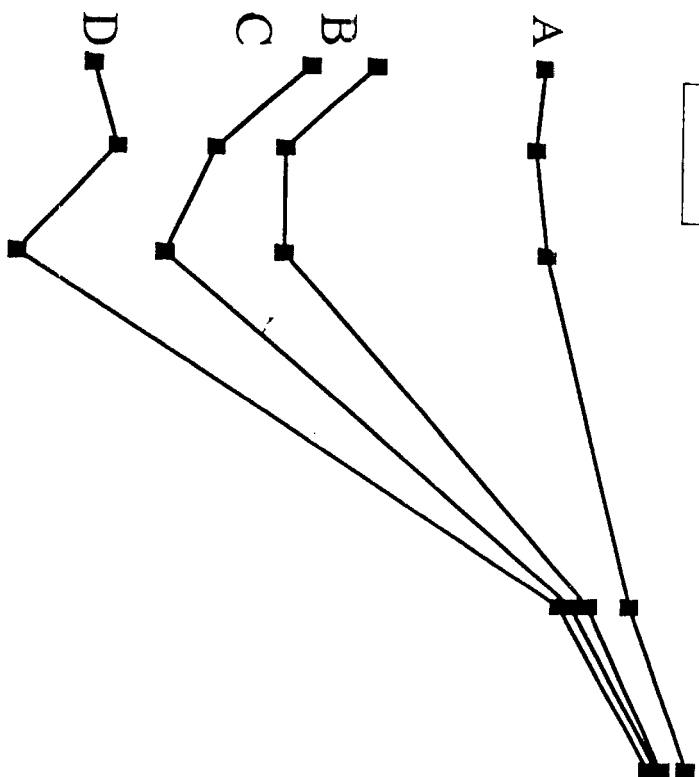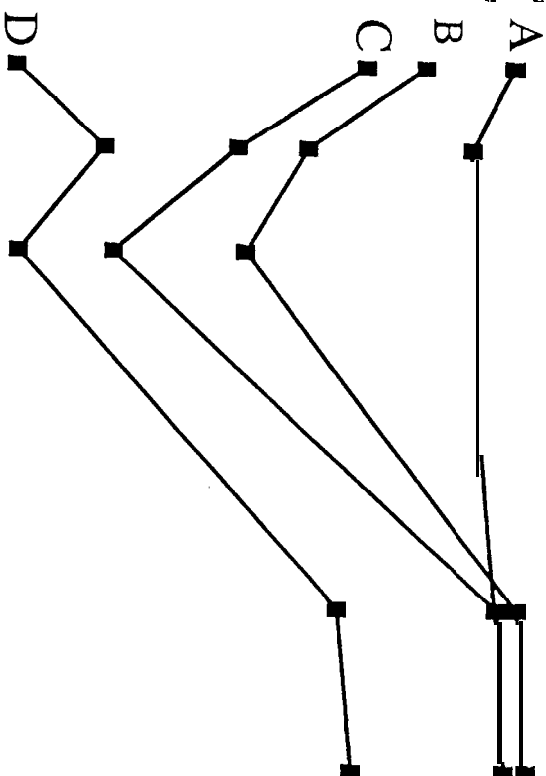
2   2.2   2.4

IMAGE

A B C D

8 9 10 11
WAVELENGTH microns

LAB

A B C D

8 9 10 11
WAVELENGTH, microns